

## MECHANICS

Original article

DOI: <https://doi.org/10.18721/JPM.17310>

### AN ANALYSIS OF THE ACCURACY OF SHORT-WAVE AND LONG-WAVE ASYMPTOTICS FOR STATIONARY LAMB WAVES IN THE ISOTROPIC LAYER

*Ya. K. Astapov, A. V. Lukin<sup>✉</sup>, I. A. Popov*

Peter the Great St. Petersburg Polytechnic University, St. Petersburg, Russia

<sup>✉</sup> [lukin\\_av@spbstu.ru](mailto:lukin_av@spbstu.ru)

**Abstract.** In the paper, the exact and asymptotic approximate solutions for symmetric and antisymmetric Lamb waves in the homogeneous isotropic elastic film have been analyzed. Using the numerical methods of the theory of continuation of solutions of nonlinear equations, the dispersion curves were calculated for waves with different variability across the layer thickness. Based on the results obtained, the nature of the displacement field and the variability of oscillation forms depending on the wave number were studied. The asymptotic correctness of the Timoshenko and Euler – Bernoulli beam models as long-wave asymptotics of Lamb waves was analyzed.

**Keywords:** Lamb waves, Euler–Bernoulli beam model, Timoshenko beam model, bifurcation theory

**Funding:** The research was supported by the Council on Grants of the President of the Russian Federation for state support of young scientists (Grant No. МК-4577.2022.1.1).

**Citation:** Astapov Ya. K., Lukin A. V., Popov I. A., An analysis of the accuracy of short-wave and long-wave asymptotics for stationary Lamb waves in the isotropic layer, St. Petersburg State Polytechnical University Journal. Physics and Mathematics. 17 (3) (2024) 105–117. DOI: <https://doi.org/10.18721/JPM.17310>

This is an open access article under the CC BY-NC 4.0 license (<https://creativecommons.org/licenses/by-nc/4.0/>)

Научная статья

УДК 534-16

DOI: <https://doi.org/10.18721/JPM.17310>

### АНАЛИЗ ТОЧНОСТИ КОРОТКОВОЛНОВЫХ И ДЛИННОВОЛНОВЫХ АСИМПТОТИК ДЛЯ СТАЦИОНАРНЫХ ВОЛН ЛЭМБА В ИЗОТРОПНОМ СЛОЕ

*Я. К. Астапов, А. В. Лукин<sup>✉</sup>, И. А. Попов*

Санкт-Петербургский политехнический университет Петра Великого, Санкт-Петербург, Россия

<sup>✉</sup> [lukin\\_av@spbstu.ru](mailto:lukin_av@spbstu.ru)

**Аннотация.** В работе анализируются точные и асимптотические приближенные решения для симметричных и антисимметричных волн Лэмба в однородном изотропном упругом слое. При помощи численного аппарата теории продолжения решений нелинейных уравнений вычислены дисперсионные кривые для волн с различной изменяемостью по толщине слоя. На основе полученных результатов исследован характер поля перемещений и изменчивость форм колебаний в зависимости от величины волнового числа. Проведен анализ асимптотической корректности балочных моделей Тимошенко, Бернулли – Эйлера как длинноволновых асимптотик волн Лэмба.

**Ключевые слова:** волны Лэмба, модель балки Бернулли – Эйлера, модель балки Тимошенко, теория бифуркации

**Финансирование:** Работа выполнена при поддержке Совета по грантам Президента Российской Федерации для государственной поддержки молодых российских ученых (грант № МК4577.2022.1.1-).

**Ссылка для цитирования:** Астапов Я. К., Лукин А. В., Попов И. А. Анализ точности коротковолновых и длинноволновых асимптотик для стационарных волн Лэмба в изотропном слое // Научно-технические ведомости СПбГПУ. Физико-математические науки. 2024. Т. 17. № 3. С. 105–117. DOI: <https://doi.org/10.18721/JPM.17310>

Статья открытого доступа, распространяемая по лицензии CC BY-NC 4.0 (<https://creativecommons.org/licenses/by-nc/4.0/>)

### Introduction

Modern requirements for new generation 5G TV and radio communication devices necessitate expanding the frequency range used to receive and transmit the signal. The ultrahigh frequency (UHF) range (over 6 GHz) is considered for this purpose. However, modern models of resonators used to generate and filter signals cannot operate at such high frequencies. Therefore, new models that ensure uninterrupted communication in a given range must be designed. While there are many types of elastic waves in solids, Lamb waves generated in thin layers show promise for solving this problem [1]. It was established that certain wave modes of this type are capable of transmitting microwave signal with minimal losses [2–4]. Numerous studies have considered this subject [5]. The design of electroacoustic transducers in a given frequency range under the constraints of microsystem technology relies on multiparametric calculations to select the optimal resonator configuration: layer thickness, electrode gap in interdigital transducers, orientation of a single crystal, etc. [6–9]. Furthermore, it is necessary to determine the specific operating modes of resonator vibrations (their variability across the layer thickness), providing the required values of the electromechanical coupling factor, additionally allowing for effective excitation by an electric field. The solutions for such problems can be obtained by combining qualitative analytical estimations based on simplified models with detailed numerical calculations based on verified procedures.

This paper reports on the qualitative study of stationary elastic Lamb waves in a homogeneous isotropic elastic layer. We performed a rigorous analytical study of the dispersion curves of symmetric and antisymmetric Lamb waves, their asymptotic analysis, direct numerical solution of the problem and comparison with known models of structural mechanics.

### Mathematical model used

A homogeneous isotropic elastic layer oriented along the  $x_1$  axis in length and along the  $x_3$  axis in thickness is considered. The layer is assumed to be infinitely long with a thickness of  $2h$  ( $-h \leq x_3 \leq h$ ). The problem is considered in a plane strain statement. The schematic of the model is shown in Fig. 1.

A system of elastodynamics equations is considered:

$$\mu \nabla^2 \mathbf{u} + (\lambda + \mu) \text{grad}(\text{div}(\mathbf{u})) = \rho \ddot{\mathbf{u}}, \quad (1)$$

where  $\lambda$ ,  $\mu$  are the Lamé parameters,  $\rho$  is the density of the material,  $\mathbf{u}$  is the vector of the displacement field.

It is known [10] that representing system of equations (1) as

$$\mathbf{u} = \text{grad } \Phi + \text{rot } \psi \quad (2)$$

reduces it to the system of wave equations:



$$\frac{\tanh(\tilde{k}\sqrt{1-\delta^2\tilde{c}^2})}{\tanh(\tilde{k}\sqrt{1-\tilde{c}^2})} = \frac{(2-\tilde{c}^2)^2}{4\sqrt{1-\delta^2\tilde{c}^2}\sqrt{1-\tilde{c}^2}}, \quad (10)$$

if we introduce the following notations:

$$\tilde{k} = kh, \quad \tilde{c} = \frac{c}{c_2}, \quad \tilde{\omega} = \tilde{k} \cdot \tilde{c} = \frac{khc}{c_2}, \quad \delta = \frac{c_2}{c_1}. \quad (11)$$

Eq. (10) is transcendental with respect to the dimensionless phase velocity of the wave and the wavenumber. Limiting cases are known for Eq. (10) [11].

Consider the first limiting case when the traveling wave length is significantly greater than the plate thickness, i.e.,  $\lambda = 2\pi/k \gg 2h$ . Then the hyperbolic tangents of Eq. (10) are replaced by their arguments. Transforming Eq. (10), we obtain:

$$4(1-\delta^2\tilde{c}^2) = (2-\tilde{c}^2),$$

$$\tilde{c} = 2\sqrt{1-\delta^2}.$$

Let  $\mu = \lambda$  (i.e., Poisson's ratio  $\nu = 1/4$ ). Then we can establish that  $\delta^2 = 1/3$ . As a result, we obtain the threshold value of the dimensionless phase velocity:

$$\tilde{c} = \tilde{c}_p = 2\sqrt{2/3} \approx 1.633\dots \quad (12)$$

Consider the second limiting case, when the wavelength is much smaller than the thickness, i.e.,  $\lambda = 2\pi/k \ll 2h$ ; then the tangent ratio can be assumed to equal unity. Transformation of Eq. (10) takes the following form:

$$(2-\tilde{c}^2)^2 = 4\sqrt{1-\delta^2\tilde{c}^2}\sqrt{1-\tilde{c}^2}. \quad (13)$$

This equality is the characteristic equation of Rayleigh surface waves [10]. The value of the phase velocity for  $\delta^2 = 1/3$  is

$$\tilde{c} = \tilde{c}_R \approx 0.9194\dots \quad (14)$$

The solution of transcendental equation (10) was obtained by the numerical framework from the theory of continuation of solutions of nonlinear equations [11]. Fig. 2 shows the dispersion curves and the dependence of the phase velocity on the wavenumber for the first three branches of the wave solution at different values of Poisson's ratio.

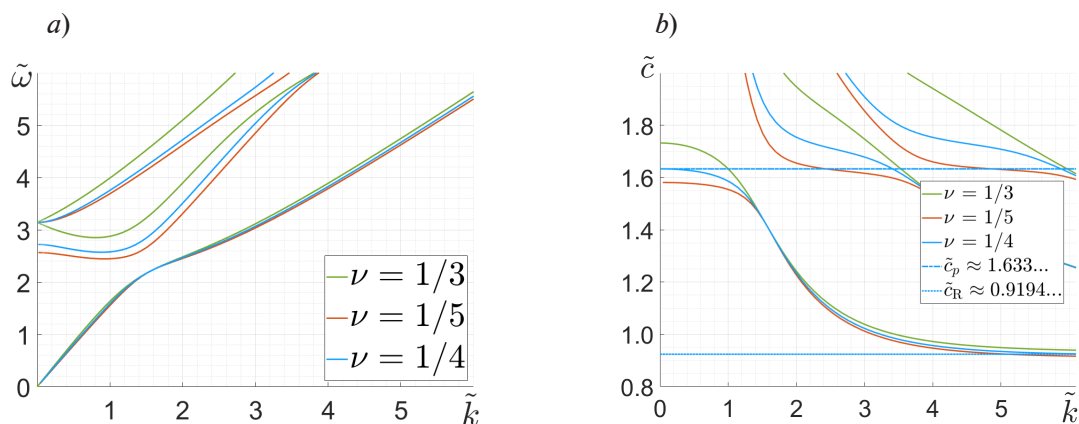


Fig. 2. Graphs for solution of Eq. (10): dispersion curves of symmetric Lamb waves (a); dependences of phase velocity (b) on wavenumber



Fig. 2,*b* confirms the correctness of both asymptotic estimates (long-wave and short-wave).

The fields of displacement in the layer were constructed for the results obtained. Their form was obtained by substituting solution (7) into Eq. (2). Fig. 3 shows the displacement fields of the first three wave modes at different values of the wavenumber: near the long-wave approximation ( $\tilde{k} = 1$ ) (*a*); for an arbitrary value ( $\tilde{k} = 2$ ) (*b*); near the short-wave approximation ( $\tilde{k} = 6$ ) (*c*). The displacement fields are constructed for a segment of an infinitely long plate (see Fig. 1); its segment =  $2\pi/k$  corresponds to one period of wave oscillation. This value is plotted along the abscissa, the thickness of the plate is plotted along the ordinate.

The colored curves visualize the vertical displacements  $u_3$ , the grid visualizes the horizontal displacements  $u_1$ .

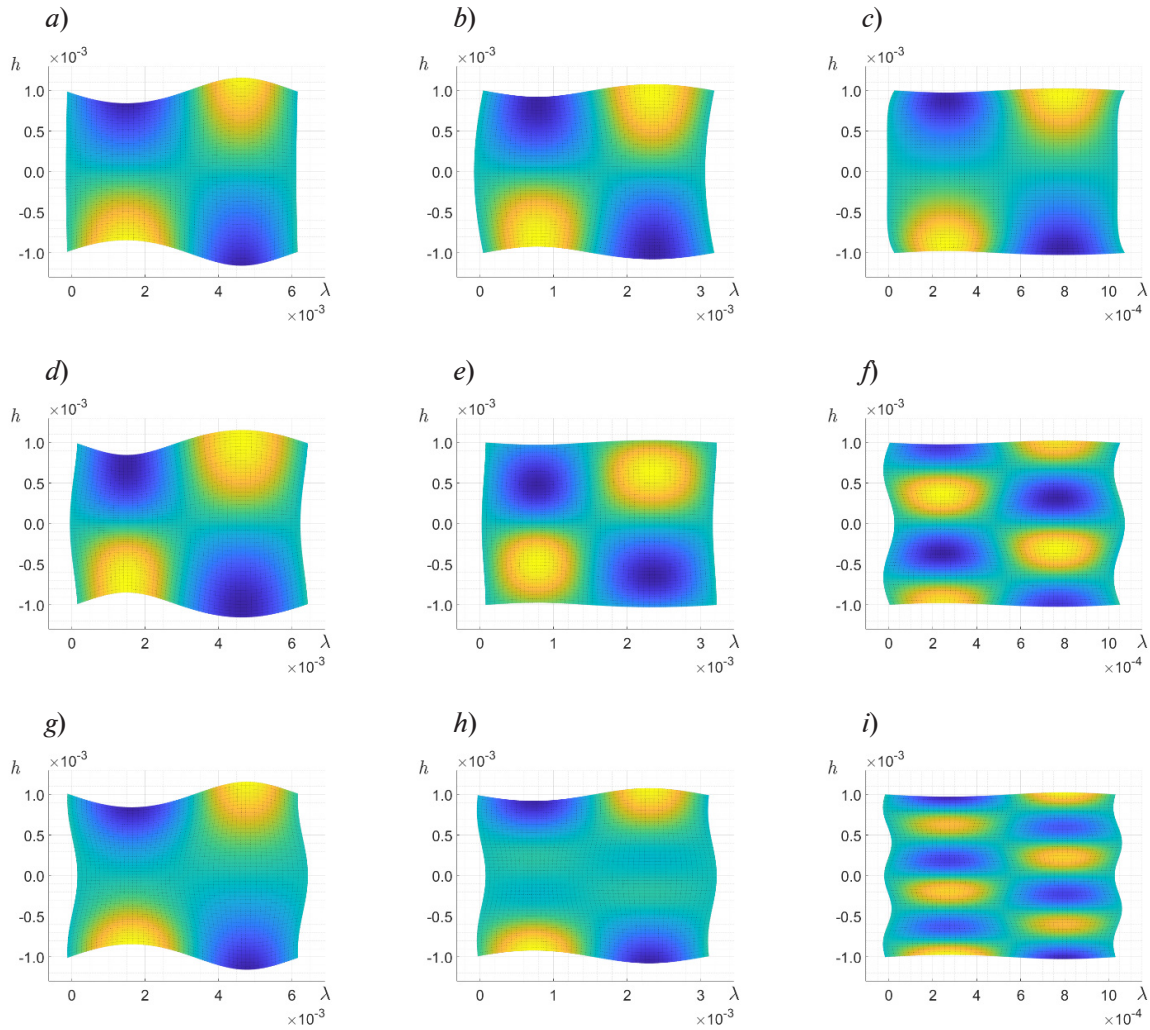


Fig. 3. Displacement fields for first three modes ( $S_0, S_1, S_2$ ) of symmetric waves at different wavenumbers  $\tilde{k}$ : mode  $S_0$  (*a, b, c*); mode  $S_1$  (*d, e, f*); mode  $S_2$  (*g, h, i*)

Analyzing the graphs, we can conclude that the number of fixed nodes increases with an increase in the value of the wavenumber in the layer. Notably, the point mass describes an elliptic trajectory during the oscillation period [12], while the behavior of the plate's eigenmode with increasing wavenumber is somewhat unexpected. This generates the additional problem of analyzing the variability of the wave mode with varying wavenumber. The results for the first three modes of symmetric waves are shown in Fig. 4.

As evident from Fig. 4,*b*, the behavior of the displacement field  $u_3$  remains almost unchanged with varying wavenumber: a midline with no displacements is observed, while upper and lower half-spaces of the plate make antiphase oscillations along the  $x_3$  axis. On the other hand, the

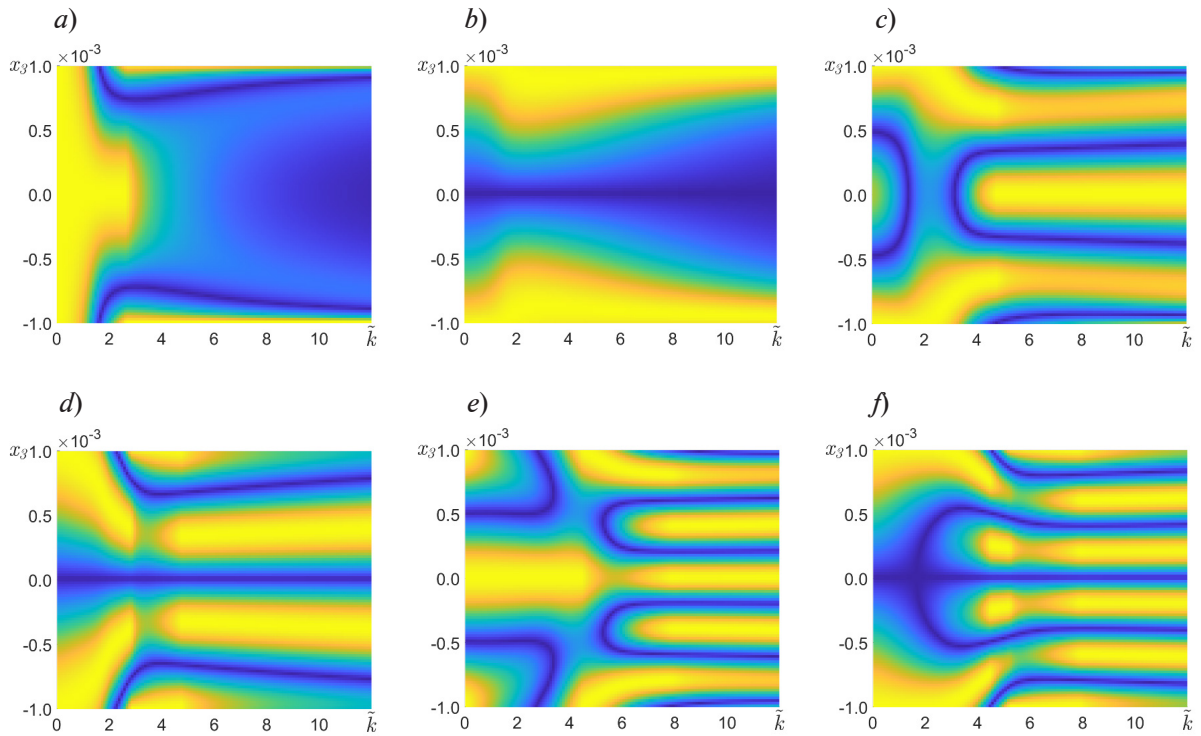


Fig. 4. Dependences of displacement fields  $u_1$  (a, c, e) and  $u_3$  (b, d, f) for three branches of solutions ( $S_0$ ,  $S_1$ ,  $S_2$ ) of symmetric wave versus wavenumber; branch  $S_0$  (a, b); branch  $S_1$  (c, d); branch  $S_2$  (e, f)

behavior of displacements  $u_1$  changes: initially, strictly longitudinal oscillations in the horizontal direction are observed, but as the wavenumber  $\tilde{k}$  approaches 1.75, a new node appears, so that antiphase oscillations in the horizontal direction are observed in the cross-section. It is also clear that the condition of the short-wave approximation is satisfied, namely, strong damping of oscillations in the bulk of the layer is observed with an increase in the wavenumber. The behavior of the second (see Fig. 4, c, d) and third (Fig. 4, e, f) wave modes changes dramatically in the long-wave approximation. On the other hand, this behavior is preserved for the wavenumber  $\tilde{k} > 6$ .

#### Antisymmetric waves

Consider the case of antisymmetric waves. A wave is called antisymmetric when the particles of the medium make antisymmetric horizontal and symmetric vertical movements relative to the cross-section midline. The vertical oscillations of the half-spaces occur in one direction, and the midline is deformed. Solution (4) takes the following form:

$$\begin{aligned} \Phi &= A \sinh(\nu_1 x_3) e^{ik(x_1 - ct)}, \\ \psi &= D \cosh(\nu_2 x_3) e^{ik(x_1 - ct)}. \end{aligned} \quad (15)$$

System of equations (8) is written as follows for the obtained solutions (15):

$$\begin{cases} 2i\beta_1 \cosh(\nu_1 h) A - (1 + \beta_2^2) \cosh(\nu_2 h) D = 0, \\ [(\lambda + 2\mu)\beta_1^2 - \lambda] \sinh(\nu_1 h) A + 2i\mu\beta_2 \sinh(\nu_2 h) D = 0. \end{cases} \quad (16)$$

If we take the determinant of system (16) and perform non-dimensionalization (11), we obtain the following transcendental equation:

$$\frac{\tanh(\nu_1 h)}{\tanh(\nu_2 h)} = \frac{4\beta_1\beta_2}{(1 + \beta_2^2)^2}. \quad (17)$$

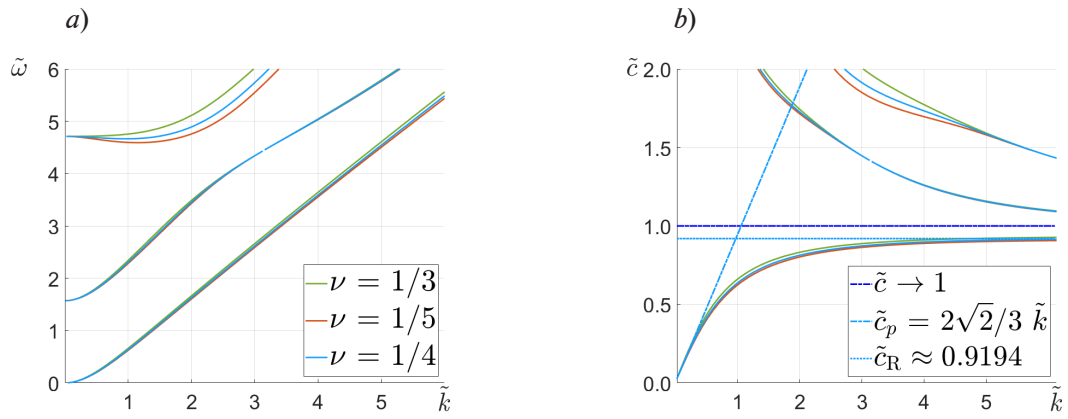


Fig. 5. Graphs for solution of Eq. (17): dispersion curves of antisymmetric Lamb waves (a); dependences of phase velocity on wavenumber (b)

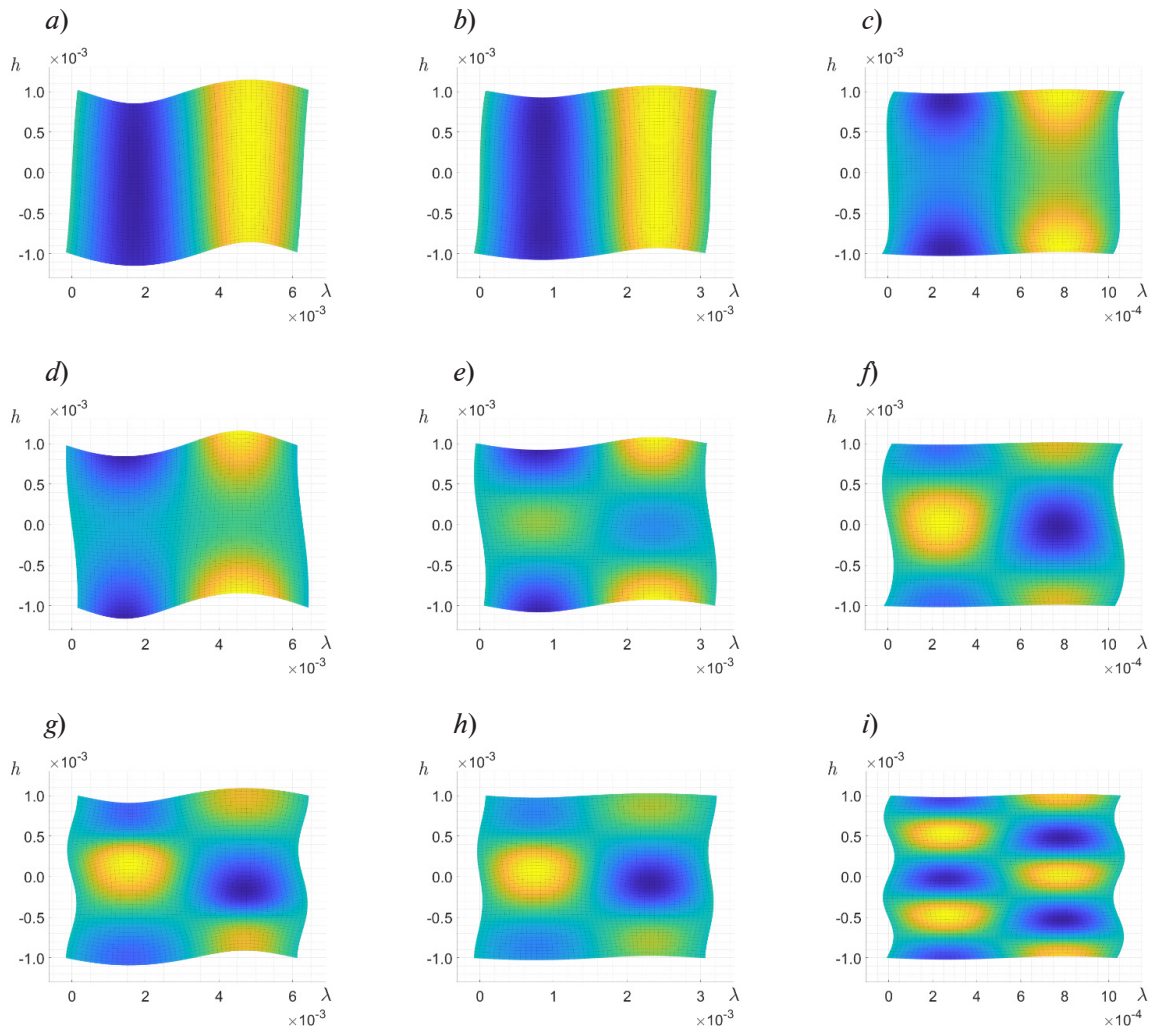


Fig. 6. Displacement fields of first three modes ( $A_0$ ,  $A_1$ ,  $A_2$ ) of antisymmetric waves at different wavenumbers  $\tilde{k}$ : mode  $A_0$  (a, b, c); mode  $A_1$  (d, e, f); mode  $A_2$  (g, h, i)

Consider the limiting cases for Eq. (17). If the wavelength significantly exceeds the thickness of the layer, the inequality  $\tilde{c} < 1 < 1/\delta$  holds true. After all the transformations (in accordance with the data presented in [10]), the transcendental equation takes the following form:

$$\tilde{c}^2 = \frac{4}{3} \tilde{k}^2 (1 - \delta^2). \tag{18}$$

Let  $\mu = \lambda$  (i.e.,  $\nu = 1/4$ ); then  $\delta^2 = 1/3$ , which implies that

$$\tilde{c}_p = \frac{2\sqrt{2}}{3} \tilde{k}. \tag{19}$$

Thus, we obtain a linear asymptote for the long-wave approximation from Eq. (19).

Consider another limiting case where the wavelength is much smaller than the plate thickness and the inequality  $\tilde{c} < 1 < 1/\delta$  holds true. Transforming Eq. (17), we arrive again at the characteristic equation for Rayleigh surface waves (13), (14). The phase velocity for case  $\tilde{c} > 1$  tends to 1.

Fig. 5 shows the dispersion curves of antisymmetric oscillations and the dependence of phase velocity on wavenumber. Evidently (see Fig. 5, *b*), the results obtained for the first branch of antisymmetric waves satisfy both approximations. It is assumed [10] that the phase velocity for the remaining modes tends to unity in the case of the short-wave approximation.

The same as for symmetric oscillations, displacement fields of antisymmetric oscillations were constructed (Fig. 6).

As seen from Fig. 6, *a*, the first mode of antisymmetric oscillations resembles bending vibrations of a beam. Also, similar to the symmetric case, a change in the wave mode is observed with an increasing wavenumber. Based on this, we analyzed the variability of the wave mode with varying wavenumber (Fig. 7).

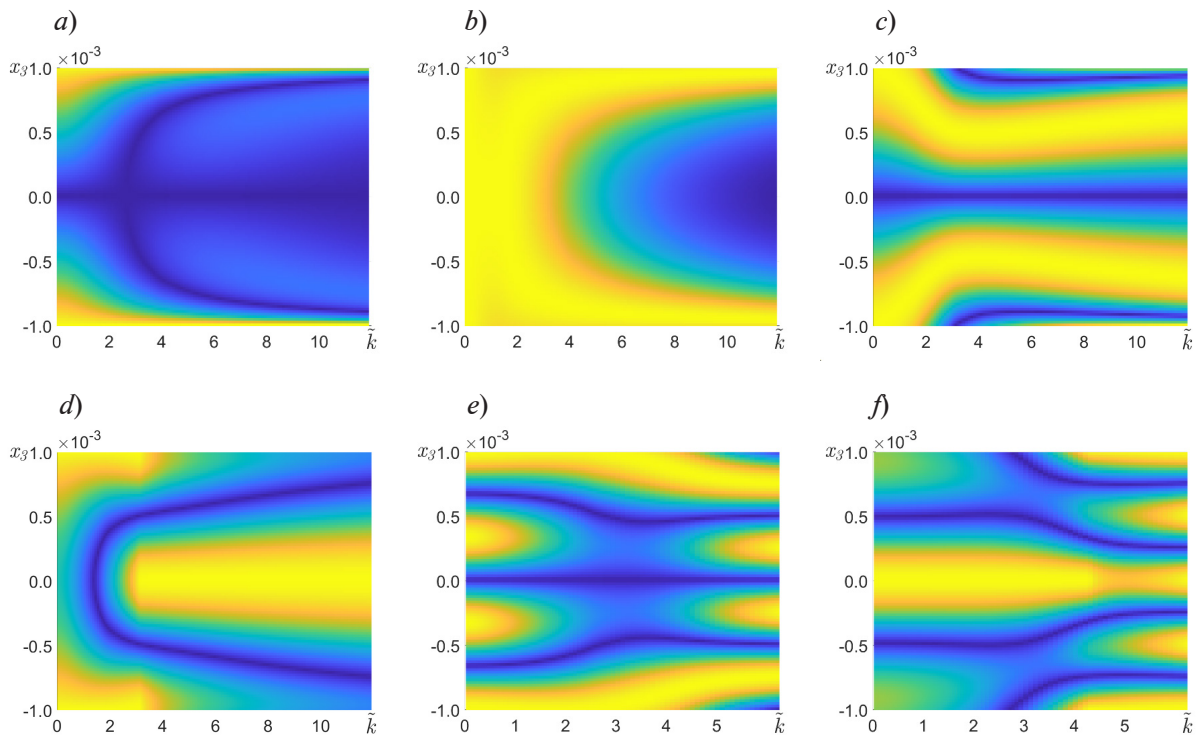


Fig. 7. Dependences of displacement fields  $u_1$  (*a, c, e*) and  $u_3$  (*b, d, f*) for three branches of solutions ( $A_0, A_1, A_2$ ) of antisymmetric wave versus wavenumber; branch  $A_0$  (*a, b*); branch  $A_1$  (*c, d*); branch  $A_2$  (*e, f*)



It is clear from Fig. 7,*b* that the amplitude of oscillations dampens rapidly in the bulk of the layer with increasing wavenumber, which corresponds to the short-wave approximation. Additionally, at low values of the parameter  $\tilde{k}$ , oscillations are performed by the entire cross-section, whereas in the short-wave case, oscillations occur in the upper and lower half-spaces of the plate, without actually interacting with each other [13]. This effect is explained by the type of wave, since at high values of the wavenumber (as mentioned above), the wave becomes similar in nature to a Rayleigh surface wave, characterized by rapid damping in the half-space [10]. In addition, an interesting branching effect of the nodal curve is observed in Fig. 7,*a*. Apparently, the branching occurs at the same wavenumbers at which the aforementioned antisymmetric wave is divided into two components formed in the upper and lower half-spaces of the plate. Based on these considerations, it can be expected that similar branchings will no longer be observed with a further increase in the wavenumber: on the contrary, complete damping of oscillations should happen in the bulk of the material.

### Analysis of asymptotic correctness of beam models

As noted above, the long-wave approximation of the first mode of the antisymmetric wave resembles in form the transverse vibrations of a beam. Two models of bending vibrations of a beam are common and well-studied in engineering practice: the Euler–Bernoulli beam and the Timoshenko beam. In view of this observation, it is advisable to compare the results obtained with the dispersion relations for these models.

It is known [12] that the problem for the Euler–Bernoulli beam model in the case of a hinged support is determined by the system:

$$\begin{cases} EI \frac{\partial^4 w}{\partial x^4} + \frac{\rho}{A} \frac{\partial^2 w}{\partial t^2} = 0, & (0 < x < l) \\ w(x, t) = 0, \quad \frac{\partial^2 w}{\partial x^2} = 0, & (x = 0, l) \\ w(x, 0) = W(x), \end{cases} \quad (20)$$

where  $w$  is the vertical displacement,  $E$  is Young's modulus,  $I$  is the moment of inertia of the cross-section,  $A$  is the cross-sectional area,  $W(x)$  are the initial displacement distributions,  $\rho$  is the surface density,  $l$  is the length of the beam.

The solution of system (20) can be represented as an infinite sum of traveling waves:

$$w(x, t) = \frac{1}{2} \sum_{n=0}^{\infty} A_n \left[ \sin\left(\frac{n\pi}{l}x - \omega_n t\right) + \sin\left(\frac{n\pi}{l}x + \omega_n t\right) \right], \quad (21)$$

where the frequency  $\omega_n$  is determined by the expression

$$\omega_n = (n\pi/l)^2 \sqrt{EIA/\rho}.$$

The wavelength in this case is  $\lambda_n = 2l/n$ . Therefore, the phase velocity is expressed as

$$c_n = \frac{\omega_n \lambda_n}{2\pi} = n\pi \sqrt{\frac{EIA}{\rho l^2}}. \quad (22)$$

For the Timoshenko beam model, the system takes the form:

$$\begin{cases} EI \frac{\partial^2 \psi}{\partial x^2} + k'AG \left( \frac{\partial w}{\partial x} - \psi \right) - \frac{\rho I}{A^2} \frac{\partial^2 \psi}{\partial t^2} = 0, \\ k'AG \left( \frac{\partial^2 w}{\partial x^2} - \frac{\partial \psi}{\partial x} \right) - \frac{\rho}{A} \frac{\partial^2 w}{\partial t^2} = 0, \\ w(x, t) = \frac{\partial}{\partial x} \psi(x, t) = 0 \quad (x = 0, l), \end{cases} \quad (23)$$

where  $\psi$  is the bending rotation,  $k' = 5/6$  is the correction factor for the rectangular cross-section,  $G$  is the shear modulus.

The expression for the eigenfrequency spectrum follows from system (23):

$$\tilde{\omega}_n^2 = \frac{(\eta^2 + \alpha^2)n^2\pi^2 + 1 \pm \sqrt{((\eta^2 + \alpha^2)n^2\pi^2 + 1)^2 - 2\eta^2\alpha^2n^4\pi^4}}{2\eta^2\alpha^2}, \quad (24)$$

where  $\tilde{\omega}_n$  is the dimensionless frequency,  $\tilde{\omega}_n^2 = \omega^2(\rho l^4)/(EIA)$ ;  $\eta$  is a dimensionless parameter expressing the ratio between bending and shear stiffness,  $\eta^2 = (EI)/(k'AGl^2)$ ;  $\alpha$  is a dimensionless parameter expressing the ratio between the forces of inertia of the cross-section with respect to rotation and transverse displacement,  $\alpha^2 = I/(Al^2)$ .

Eq. (24) gives two branches of solutions for bending ( $\tilde{\omega}_{n,1}$ ) and shear ( $\tilde{\omega}_{n,2}$ ) vibrations.

It was of interest to build finite element (FE) models of Euler–Bernoulli and Timoshenko beams. The models were constructed in the COMSOL Multiphysics package. For comparison, Fig. 8 shows the results of analytical and FE modeling of the Euler–Bernoulli beam and the Timoshenko beam, as well as the previously presented calculation results using the Lamb elastic wave model in a thin layer.

Analysis of the data in Fig. 8 shows that the lower branch of the solution for the Timoshenko beam model coincides with the first branch of the wave solution of antisymmetric Lamb waves. We should note that this is not a consistent pattern. As noted above, the phase velocity of the lower branch of the Lamb wave solution in the short-wave approximation tends to the phase velocity of Rayleigh surface waves  $c_R$ , which, in turn, depends on the value of Poisson’s ratio (14). At the same time, the phase velocity of the wave for the Timoshenko beam model tends to the velocity of transverse oscillations  $c_T = \sqrt{k'G/\rho}$  with an increase in the wavenumber. In dimensionless form, these asymptotics are the result of taking the square root of the correction factor  $k'$ .

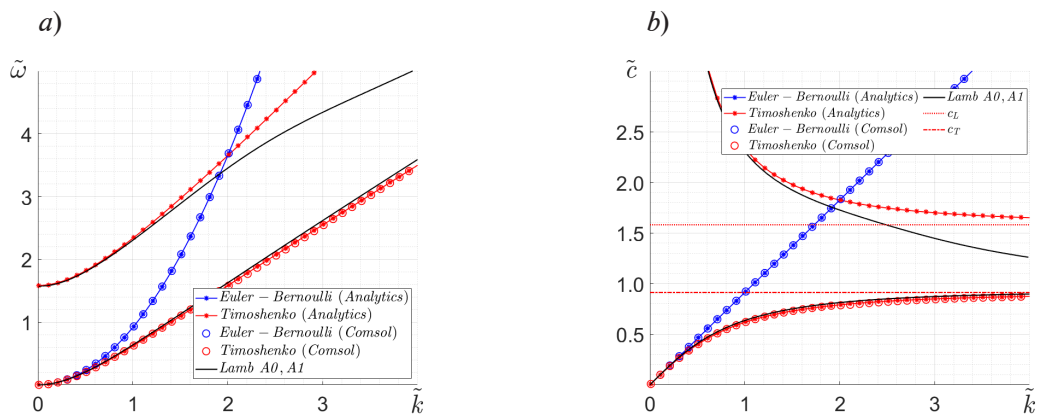


Fig. 8. Comparison of calculated results for three models: Euler–Bernoulli beams, Timoshenko beams and elastic Lamb waves; dispersion curves (a), dependences of phase velocity on wavenumber (b)

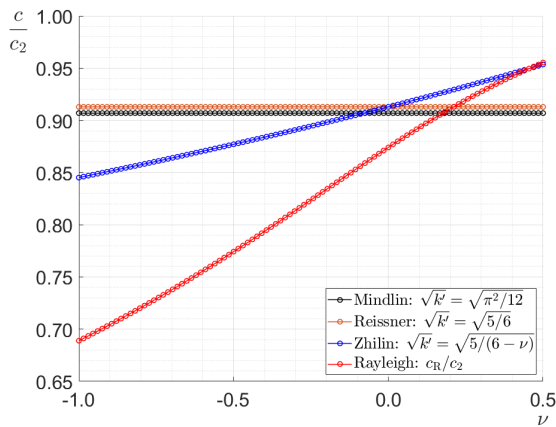


Fig. 9. Comparison of dependences of threshold phase velocities on Poisson's ratio

correction factor  $k'$ . These proposals do not coincide with the investigated Rayleigh surface wave model. There are, however, certain values of Poisson's ratio at which the asymptotics coincide.

Based on this, we can conclude that coincidence of the characteristics of elastic Lamb waves and waves in the Timoshenko beam is observed only for a long-wave approximation, while the results diverge if the dimensionless wavenumber  $\tilde{k} = k \cdot h \approx 1$ .

### Conclusion

We performed a qualitative analytical study of stationary Lamb waves in a homogeneous isotropic thin layer. Dispersion curves and phase velocity dependences on the wavenumber were constructed for symmetric and antisymmetric waves in accordance with the obtained solutions. The displacement and variability fields were calculated for the wave mode of the first branch of the wave solution with variable value of the wavenumber. The characteristics of antisymmetric Lamb waves were compared with the wave characteristics of Euler–Bernoulli and Timoshenko beams. The data help determine the accuracy of long-wave and short-wave asymptotic approximations for symmetric and antisymmetric Lamb waves, including approximations based on the application of beam models of structural mechanics.

Our findings can serve as a basis for verification of numerical methods of wave mechanics used in modeling wave processes in electroacoustic devices.

### REFERENCES

1. Lu R., Gong S., RF acoustic microsystems based on suspended lithium niobate thin films: Advances and outlook, *J. Micromech. Microeng.* 31 (11) (2021) 114001.
2. Yang Y., Lu R., Gao L., Gong S., 10–60-GHz Electromechanical resonators using thin-film lithium niobate, *IEEE Trans. Microw. Theory Techn.* 68 (12) (2020) 5211–5220.
3. Yang Y., Lu R., Gong S., Scaling acoustic filters towards 5G, *Proc. 2018 IEEE International Electron Devices Meeting (IEDM)*, 01–05 Dec., San Francisco, CA, USA (2018) 39.6.1–39.6.4.
4. Yang Y., Gao L., Gong S., X-band miniature filters using lithium niobate acoustic resonators and bandwidth widening technique, *IEEE Trans. Microw. Theory Techn.* 69 (3) (2021) 1602–1610.
5. Wu J., Zhang Sh., Zhang L., et al., Exploring low-loss surface acoustic wave devices on heterogeneous substrates, *IEEE Trans. Ultrason. Ferroelectr. Freq. Control.* 69 (8) (2022) 2579–2584.
6. Naumenko N. F., Optimal orientations of LiTaO<sub>3</sub> for application in plate mode resonators, *J. Appl. Phys.* 118 (3) (2015) 034505.
7. Naumenko N. F., Laterally excited bulk acoustic resonators (XBARs): Optimization method and application to resonators on LiTaO<sub>3</sub>, *Proc. 2022 IEEE MTT-S Int. Conf. Microwave Acoustics and Mechanics (IC-MAM)*. 18–20 July 2022, Munich, Germany (2022) 70–73.
8. Naumenko N. F., Advanced numerical technique for analysis of surface and bulk acoustic waves in resonators using periodic metal gratings, *J. Appl. Phys.* 116 (10) (2014) 104503.

9. **Naumenko N. F.**, Temperature behavior of SAW resonators based on LiNbO<sub>3</sub>/Quartz and LiTaO<sub>3</sub>/Quartz substrates, *IEEE Trans. Ultrason. Ferroelectr. Freq. Control.* 68 (11) (2021) 3430–3437.
10. **Novatski V.**, *Teoriya uprugosti [Elasticity theory]*, Mir Publishing, Moscow, 1975 (in Russian).
11. **Govaerts W., Kuznetsov Yu. A., Meijer H.G.E., et al.**, *MATCONT: Continuation toolbox for ODEs in Matlab*, Utrecht University, Utrecht (The Netherlands), 2019.
12. **Gérardin, M., Rixen D. J.**, *Mechanical vibrations: Theory and application to structural dynamics.* 3-rd Ed., John Willey and Sons, Chichester (West Sussex, UK), 2015.
13. **Biryukov S. V., Gulyaev Yu. V., Krylov V. V., Plessky V. P.**, *Surface acoustic waves in inhomogeneous media (Springer Series on Wave Phenomena, Vol. 20)*, Springer-Verlag, Berlin Heidelberg, 1995.
14. **Zhilin P. A.**, *Prikladnaya Mehanika: Osnovy teorii obolochek [Applied Mechanics: Basics of shell theory]*, Polytechnic University Publishing, Saint-Petersburg, 2006 (in Russian).

### СПИСОК ЛИТЕРАТУРЫ

1. **Lu R., Gong S.** RF acoustic microsystems based on suspended lithium niobate thin films: Advances and outlook // *Journal of Micromechanics and Microengineering.* 2021. Vol. 31. No. 11. P. 114001.
2. **Yang Y., Lu R., Gao L., Gong S.** 10–60-GHz Electromechanical resonators using thin-film lithium niobate // *IEEE Transaction on Microwave Theory and Techniques.* 2020. Vol. 68. No. 12. Pp. 5211–5220.
3. **Yang Y., Lu R., Gong S.** Scaling acoustic filters towards 5G // *Proceedings of the 2018 IEEE International Electron Devices Meeting (IEDM).* San Francisco, CA, USA. 01–05 December, 2018. Pp. 39.6.1–39.6.4.
4. **Yang Y., Gao L., Gong S.** X-band miniature filters using lithium niobate acoustic resonators and bandwidth widening technique // *IEEE Transaction on Microwave Theory and Techniques.* 2021. Vol. 69. No. 3. Pp. 1602–1610.
5. **Wu J., Zhang Sh., Zhang L., Zhou H., Zheng P., Yao H., Li Zh., Huang K., Wu T., Ou X.** Exploring low-loss surface acoustic wave devices on heterogeneous substrates // *IEEE Transactions on Ultrasonics, Ferroelectrics, and Frequency Control.* 2022. Vol. 69. No. 8. Pp. 2579–2584.
6. **Naumenko N. F.** Optimal orientations of LiTaO<sub>3</sub> for application in plate mode resonators // *Journal of Applied Physics.* 2015. Vol. 118. No. 3. P. 034505.
7. **Naumenko N. F.** Laterally excited bulk acoustic resonators (XBARs): Optimization method and application to resonators on LiTaO<sub>3</sub> // *Proceedings of the 2022 IEEE MTT-S International Conference on Microwave Acoustics and Mechanics (IC-MAM).* 18 – 20 July 2022, Munich, Germany. 2022. Pp. 70–73.
8. **Naumenko N. F.** Advanced numerical technique for analysis of surface and bulk acoustic waves in resonators using periodic metal gratings // *Journal of Applied Physics.* 2014. Vol. 116. No. 10. P. 104503.
9. **Naumenko N. F.** (2021). Temperature behavior of SAW resonators based on LiNbO<sub>3</sub>/Quartz and LiTaO<sub>3</sub>/Quartz substrates // *IEEE Transactions on Ultrasonics, Ferroelectrics, and Frequency Control.* 2021. Vol. 68. No. 11. Pp. 3430–3437.
10. **Новацкий В.** Теория упругости. Пер. с польского. М.: Мир, 1975. 872 с.
11. **Govaerts W., Kuznetsov Yu. A., Meijer H.G.E., Al-Hdaibat B., de Witte V., Dhooge A., Mestrom W., Neiryck N., Riet A. M., Sautios B.** *MATCONT: Continuation toolbox for ODEs in Matlab.* Utrecht (The Netherlands): Utrecht University, 2019. 124 p.
12. **Gérardin, M., Rixen D. J.** *Mechanical vibrations: theory and application to structural dynamics.* 3-rd edition. Chichester (West Sussex, UK): John Willey and Sons, 2015. 598 p.
13. **Бирюков С. В., Гуляев Ю. В., Крылов В. В., Плесский В. П.** *Поверхностные акустические волны в неоднородных средах.* М.: Наука. Гл. редакция физ.-мат. лит.-ры, 1991. 416 с.
14. **Жилин П. А.** *Прикладная механика: Основы теории оболочек.* СПб.: Издательство Политехнического университета, 2006.

**THE AUTHORS****ASTAPOV Yaroslav K.**

*Peter the Great St. Petersburg Polytechnic University*  
29 Politechnicheskaya St., St. Petersburg, 195251, Russia  
astapov.yaroslav.00@mail.ru  
ORCID: 0009-0008-0216-462X

**LUKIN Aleksey V.**

*Peter the Great St. Petersburg Polytechnic University*  
29 Politechnicheskaya St., St. Petersburg, 195251, Russia  
lukin\_av@spbstu.ru  
ORCID: 0000-0003-2016-8612

**POPOV Ivan A.**

*Peter the Great St. Petersburg Polytechnic University*  
29 Politechnicheskaya St., St. Petersburg, 195251, Russia  
popov\_ia@spbstu.ru  
ORCID: 0000-0003-4425-9172

**СВЕДЕНИЯ ОБ АВТОРАХ**

**АСТАПОВ Ярослав Константинович** – студент Физико-механического института Санкт-Петербургского политехнического университета Петра Великого.

195251, Россия, г. Санкт-Петербург, Политехническая ул., 29  
astapov.yaroslav.00@mail.ru  
ORCID: 0009-0008-0216-462X

**ЛУКИН Алексей Вячеславович** – кандидат физико-математических наук, доцент Высшей школы механики и процессов управления Санкт-Петербургского политехнического университета Петра Великого.

195251, Россия, г. Санкт-Петербург, Политехническая ул., 29  
lukin\_av@spbstu.ru  
ORCID: 0000-0003-2016-8612

**ПОПОВ Иван Алексеевич** – ведущий инженер Высшей школы механики и процессов управления Санкт-Петербургского политехнического университета Петра Великого.

195251, Россия, г. Санкт-Петербург, Политехническая ул., 29  
popov\_ia@spbstu.ru  
ORCID: 0000-0003-4425-9172

*Received 31.01.2024. Approved after reviewing 22.04.2024. Accepted 22.04.2024.*

*Статья поступила в редакцию 31.01.2024. Одобрена после рецензирования 22.04.2024. Принята 22.04.2024.*